CONTRACTOR REPORT

SAND89—7154
Unlimited Release
UC—414

Dynamics of Plasma Injection Along Magnetic Field Lines in the PBFA II Plasma Opening Switch

Michael H. Frese
NumerEx
1400 Central SE, Suite 3200
Albuquerque, NM 87106-4811

Prepared by Sandia National Laboratories Albuquerque, New Mexico 87185 and Livermore, California 94550 for the United States Department of Energy under Contract DE-AC04-76DP00789

Printed November 1989

Issued by Sandia National Laboratories, operated for the United States Department of Energy by Sandia Corporation.

Available to DOE and DOE contractors from
Office of Scientific and Technical Information
PO Box 62
Oak Ridge, TN 37831

Prices available from (615) 576-8401, FTS 626-8401

Available to the public from
National Technical Information Service
US Department of Commerce
5285 Port Royal Rd
Springfield, VA 22161

NTIS price codes
Printed copy: A03
Microfiche copy: A01

SAND89-7154
Unlimited Release
Printed November 1989

Distribution
Category UC-414

Dynamics of Plasma Injection Along Magnetic Field Lines in the PBFA II Plasma Opening Switch

Michael H. Frese

NumerEx
1400 Central SE, Suite 3200
Albuquerque, New Mexico 87106-4811

Sandia Contract No. 40-0128

Contents

List of Figures

1. Summary

In the magnetically injected plasma (MIP) plasma opening switch (POS) presently under study for use on the Particle Beam Fusion Accelerator II (PBFA II), plasma is injected along an imposed poloidal field to control the position of the plasma. The magnetic field and the plasma density combine to make the Alfven velocity very high relative to the injection velocity of the plasma. In fact, the ratio of these velocities, the Alfven-Mach number of the flow, ranges from 0.001 to 0.01. Explicit computation at these low Mach numbers is exceedingly tedious, and implicit computation without a very high convergence rate scheme is little better. However, the physical effect is clear: the field lines are effectively very stiff and not subject to displacement by the plasma. The plasma motion may thus be computed by simply restricting the velocity to lie along the field. Simulations in the true experimental geometry using this approach agree qualitatively with microwave interferometry measurements of the plasma density in the experimental test stand. The agreement is quantitative, subject only to the adjustment of the unknown plasma source mass flux rate.

2. Problem Description

The POS region in PBFA II is geometrically complex, lying between two conical electrodes, and the MIP modifications further complicate the geometry. Figure 1 shows a computational grid that fits the biconic switch region and the adjacent semi-toroidal plasma source region. The accelerator power pulse travels from the adder located out of the picture to the upper right, down to the load at the lower left.

This grid[1] was generated by MACH2, a $2\frac{1}{2}$-D magnetohydrodynamics (MHD) code that creates and computes on multiblock boundary-fitted arbitrary quadrilateral grids. Further details on MACH2 may be found in [1]. The experimental region is cylindrically symmetric. The geometric flexibility and power of MACH2 makes it feasible to compute with such a relatively small number of cells, since the boundary conditions can be more accurately applied along grid lines that parallel the physical boundaries. No more spatial resolution is required, since the experimental diagnostics have even less resolution than this grid.

1 The locations of the essential points necessary to generate the computational grid were extracted from the CAD representation of actual MIP POS hardware by M. Slattery.

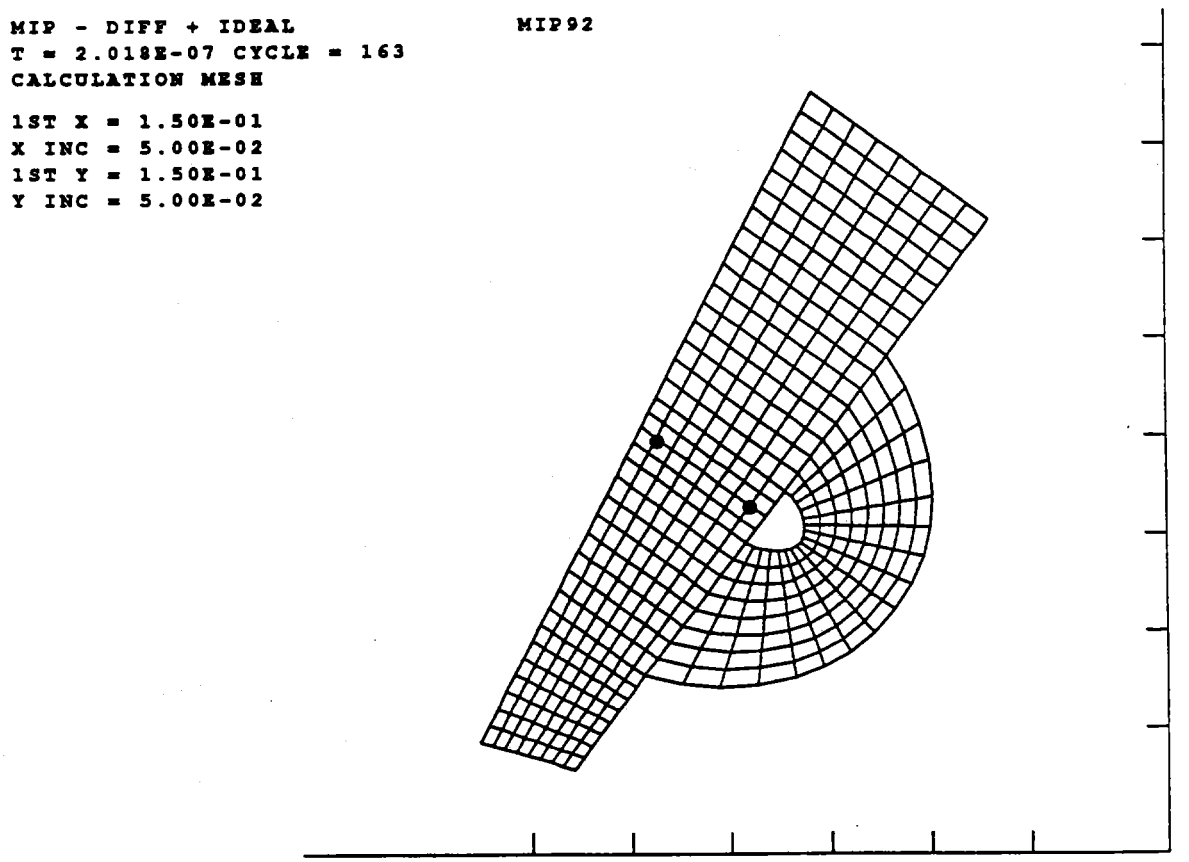

Figure 1 Computational grid fitting experimental configuration for magnetically controlled plasma injection. Dots mark location of simulation density probes.

A coil carrying from 50 to 200 kiloamp-turns of current in the toroidal direction lies in the small D-shaped hole surrounded by the computational region. The magnetic field that results from this current is shown in Figure 2. This field is computed using MACH2's multigrid implicit resistive diffusion module. The equations are advanced approximately 1000 cell diffusion times in 100 timesteps. The boundary conditions used are $\bar{n} \cdot \bar{B} = 0$ on surfaces representing conducting boundaries, and $\bar{B} = \mu_0 \frac{I}{l} \bar{t}$ on the region boundary surrounding the coil. Here I is the total current in the coil in amp-turns, l is the arc length of the curve in the computational plane surrounding the coil, and $\bar{t}$ is the tangent vector to that curve. Since l is about 6 cm, the resulting field has a maximum of approximately 2.5 T.

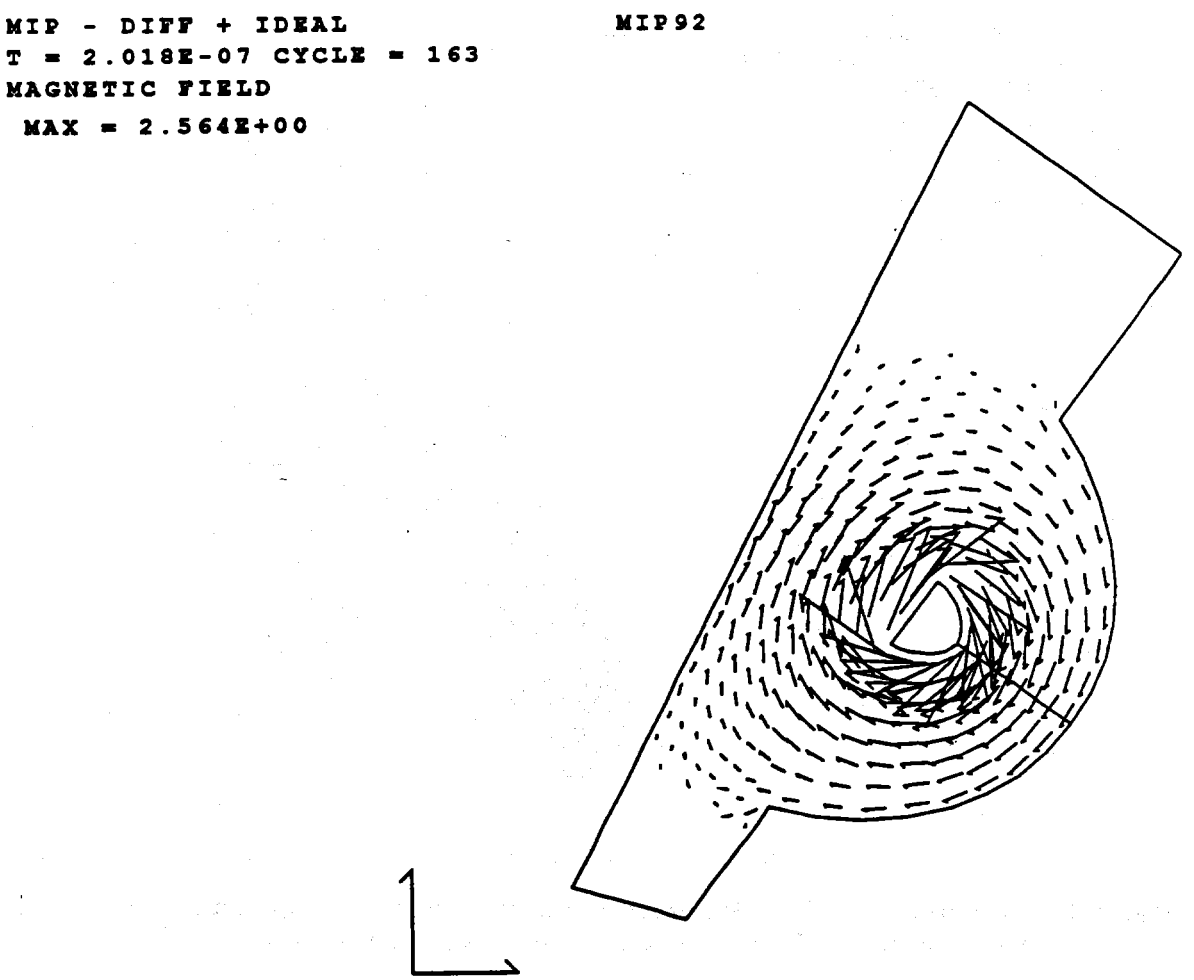

Figure 2 Magnetic field for control of plasma injection.

The injected plasma is formed by surface flashover along both upstream and downstream surfaces of flashboards shown as a line sloping down to the right in the magnetic field plot of Figure 2. It is thought to consist largely of a neutral plasma of electrons and C^{++} ions. It is believed to be ejected from the surface of the flashboards with a velocity of 10 to 20 cm/μs.

The object of this simulation study is to compute the plasma density distribution as a function of time in the POS region that results from the interaction of the magnetic field with the plasma injection pulse. Neither the accelerator power pulse or the load behavior will be considered here.

3. Computational Difficulty

As MACH2 implements resistive MHD, a one-fluid model of plasma dynamics, zero is an unsatisfactory value for the density. Hence, the computational region is initially filled completely with a neutral plasma of electron density $2 \times 10^{11} cm^{-3}$ which is approximately the density of the residual gas left by the vacuum pumping on PBFA II. This density must be sufficiently small that it has little effect on the dynamics of the injected plasma; it was chosen to be two orders of magnitude smaller than the density of the actual plasma of interest.

The velocity of Alfven waves at this density and field strength is 3×10^7 m/s. Since the grid spacing near the coil is approximately 3 mm, the transit times for these waves is only 1×10^{-10} seconds, and hence the explicit time step required would be $2 - 5 \times 10^{-11}$ seconds. For the 5 to 10 μs the plasma takes to reach and fill the switch region, the explicit full MHD computation would require $1 - 5 \times 10^5$ timesteps. For this particular problem, that is an unacceptable computer expense.

The implicit algorithm for the MHD in MACH2 can be pushed to take timesteps an order of magnitude greater, but the cost is a factor of five in computer time per timestep. Thus the payoff is only a factor of two[2], and that would still leave the problem too expensive to solve.

Clearly, the problem is that the field lines are very stiff. Transverse velocities produce large restoring forces and high opposing accelerations. In fact, the difference equations are themselves stiff in the sense of the word used in numerical analysis. There are two widely different time scales: one for the transverse plasma motions and another for the parallel. In the recognition of this lies the solution. By removing the short time scale from the problem, the computations may be made to proceed at the longer one.

[2] The reason the payoff is no better is that Jacobi iteration is employed to solve the implicit equations. A multigrid convergence acceleration scheme could pay handsome dividends here.

4. Computational Method

Since there is no toroidal field in the problem, the easiest way to remove the short time-scale motions is to simply remove all magnetohydrodynamic influence of the plasma on the magnetic field and all magnetic force on the plasma. The incorporation of a simple multiplier in the routines where these influences are applied removes them when the multiplier is set to zero. MACH2 is an Arbitrary Lagrangian/Eulerian code and hence has a time-split implementation of the transport and force equations, so that care must be taken to remove all influences. An additional routine projects the velocity onto the magnetic field everywhere within the computational region. The plasma then moves hydrodynamically under the action of its own pressure and momentum, and of course the numerical diffusion, along the magnetic field lines.

The HISTORIAN change file necessary to implement these changes in the v8801 version of MACH2 is included here as Appendix A. It is 235 lines long, but contains modifications to the circuit model unnecessary for the plasma injection simulations.

This approach produces a simulation requiring only 400 timesteps to reach 10 μs of physical time and less than 3 CRAY XMP CPU-minutes. Simulations of this size are very effective for design work.

5. Computational Results

Three simulations will be discussed in turn in the subsections to follow. The first simulation gives the best comparison with experiment. The other simulations were performed to assess the importance of the fluid pressure on the dynamics of the injected plasma. The second differs from the first only in that the inflow density is four times greater. The conditions of the third simulation are the same as the second except that the mass inflow from the downstream side of the flashboard is not present.

In general, the simulation results are dominated by the relatively shorter path lengths along the more highly curved field lines nearer the coil (see Figure 2). Plasma first arrives in the switching region immediately to the left of the coil. The plasma injected along field lines near the coil from the upstream side of the flashboard meets that from the downstream side and stagnates, creating a peak of density there at about 2 μs. The plasmas from the upstream and downstream sides on the field lines farthest from the coil do not meet in the switching region till 5 μs and the peak in the density near the cathode is at approximately this time.

An ideal gas equation of state for a C^{++} plasma is used in the simulations. The plasma pulse is simulated by specifying a constant inflow density and time varying velocity normal to the flashboards. The pulse is sinusoidal, beginning at the end of the diffusion period, and lasting a single half-period of 100 ns. The figures below that refer to the end of the plasma pulse show the velocity field and the density contours at the end of that time. In all three cases the injection velocity peaks at 10 cm/μs.

The MACH2 input file for the first simulation is included in this report as Appendix B. The input files for the others differ only slightly from that one.

The simulation results will be given using contour plots of electron density and vector plots of plasma velocity such as in Figures 3 and 4. In all plots the problem time and cycle are given in the upper left corner. In the contour plots the contour levels are linearly spaced between the maximum and minimum values of the quantity contour plotted, and are indicated in the upper left corner of the plot, along with the maximum and minimum value. The value associated with the longest vector in each vector plot is given in the upper left corner, and the length of that vector is shown in the lower left for comparison.

5.1 Low Density Case

The inflow electron density in this case is set to $5 \times 10^{13} cm^{-3}$ but because of the flow dynamics the largest values reached in the computational region are slightly less than that. The density of the injected plasma reaches only $3 \times 10^{13} cm^{-3}$. This value occurs just off the flashboard surface at the end of the plasma pulse near the

coil end of the board. The velocity peaks at approximately 8 cm/μs, also just after the end of the pulse.

The density contour lines and the velocity field of the plasma at 200 ns, the end of the injection pulse, are shown in Figures 3 and 4. The peak density at this time is located near the coil end of the flashboard. The maximum plasma velocity is approximately 8 cm/μs, and all velocities are, of course, parallel to the magnetic field.

Figures 5 and 6 show the density and velocity at 5 μs. By this time, the two plasma clouds coming from opposite sides of the flashboards are already bouncing back toward the flashboards near the coil, though they are only beginning to slow near the cathode. The double peak in the density results because the plasma that has reversed course along the field lines after meeting in the transmission line is meeting the oncoming tail of plasma.

The electron number density at the density probe locations (marked by the dots in Figure 1) is plotted versus time in Figure 7. The density near the anode peaks first, at approximately 2 μs, while the density near the cathode peaks slightly after 6 μs. The peak density near the cathode, $6 \times 10^{12} cm^{-3}$, is approximately half the peak near the anode.

For comparison, Figure 7 also shows the experimental range of density measured by Weber [2] near the cathode in the laboratory test stand using microwave interferometry. This measurement was taken approximately 2 cm downstream of the cathode simulation density probe location shown in Figure 1. The lower edge of the gray region is the density vs. time for a shot with 16 kA-turns of coil flux, and the upper edge is the density vs. time for a shot with 47 kA-turns of coil flux. These coil fluxes are significantly lower than those that will be used on PBFA II and at these levels, the measured density increases with flux. Weber reports that at other locations this increase saturates at slightly higher flux levels.

The favorable comparison of this simulation result with experiment is somewhat fortuitous, since the density of mass injection was selected rather arbitrarily. As the simulation preceded the experiment, the author submits that all congratulations on this good fortune should be conferred upon Dr. Weber and his experimental colleagues. The fact that the experiment followed the simulation is the reason that the locations of the simulation density probes differ from those of the microwave interferometry diagnostics.

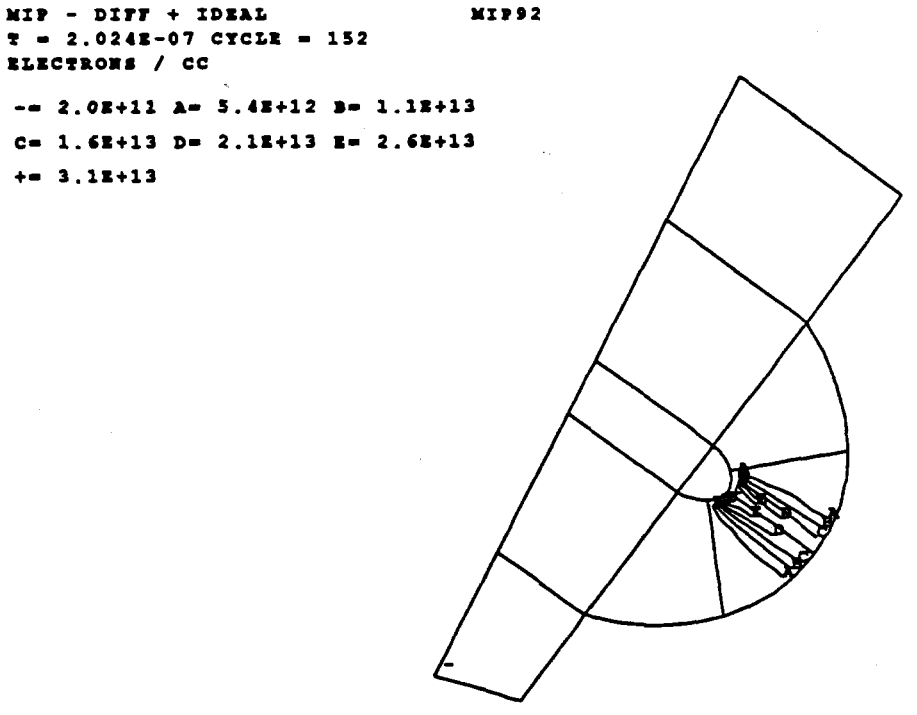

Figure 3 Density at the end of the mass injection pulse. Low density case.

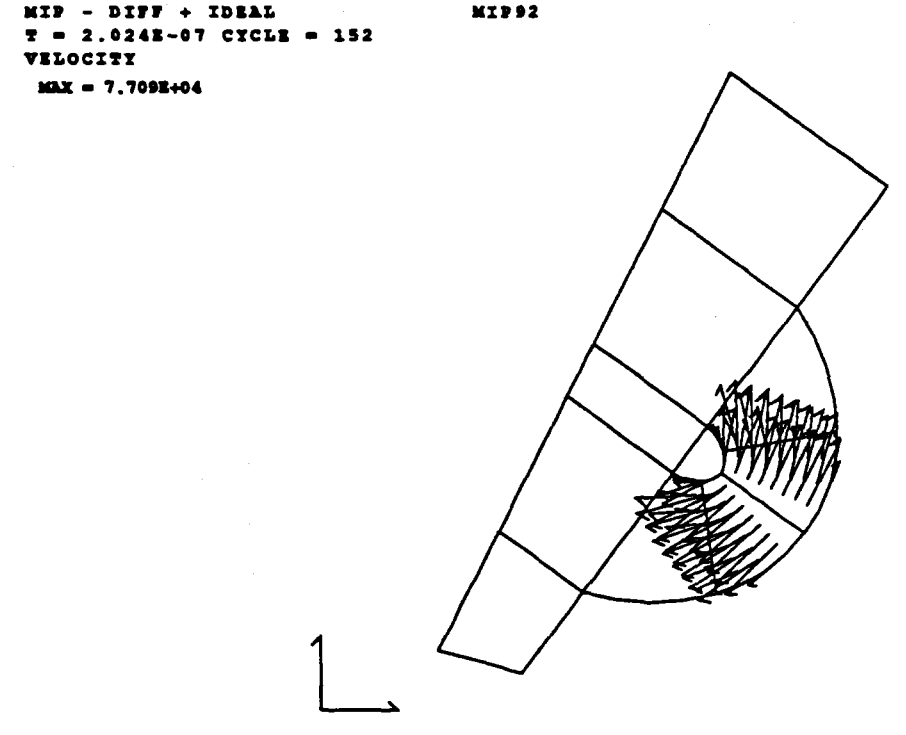

Figure 4 Velocity at the end of the mass injection pulse. Low density case.

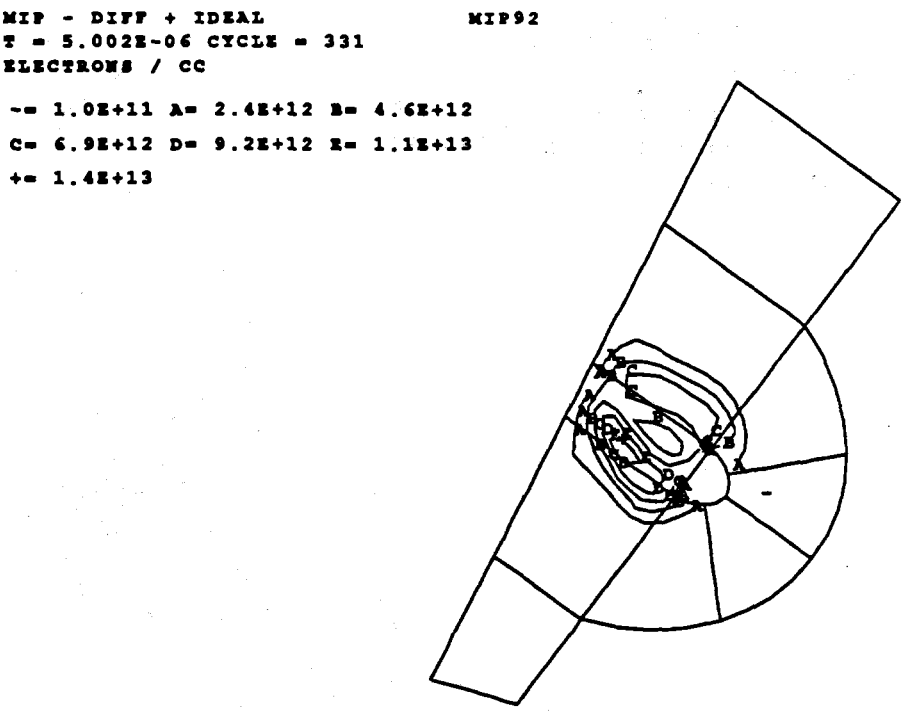

Figure 5 Density at 5 μs after the start of the mass injection pulse. Low density case.

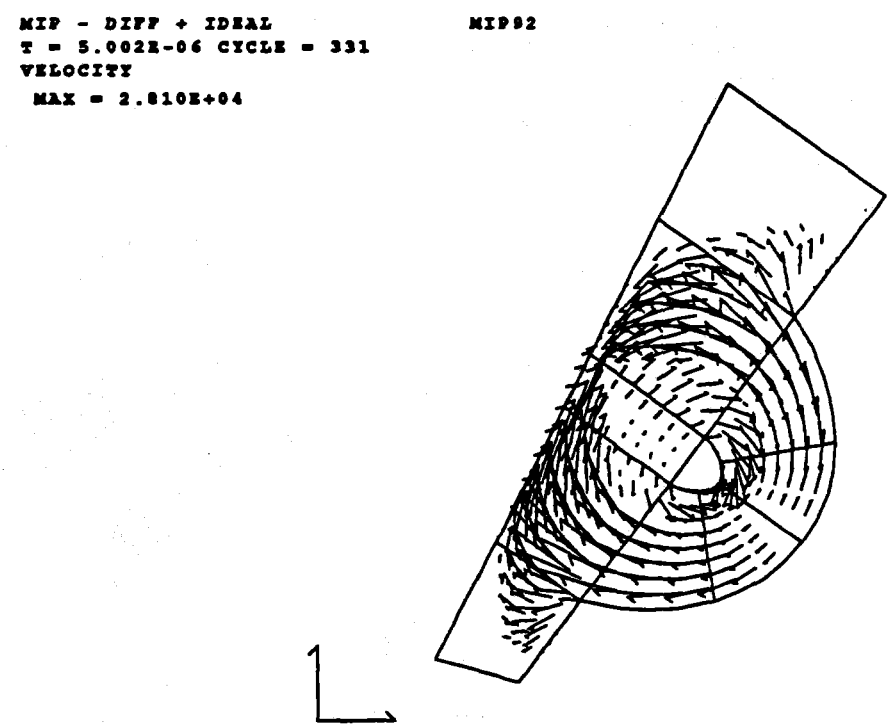

Figure 6 Velocity at 5 μs after the start of the mass injection pulse. Low density case.

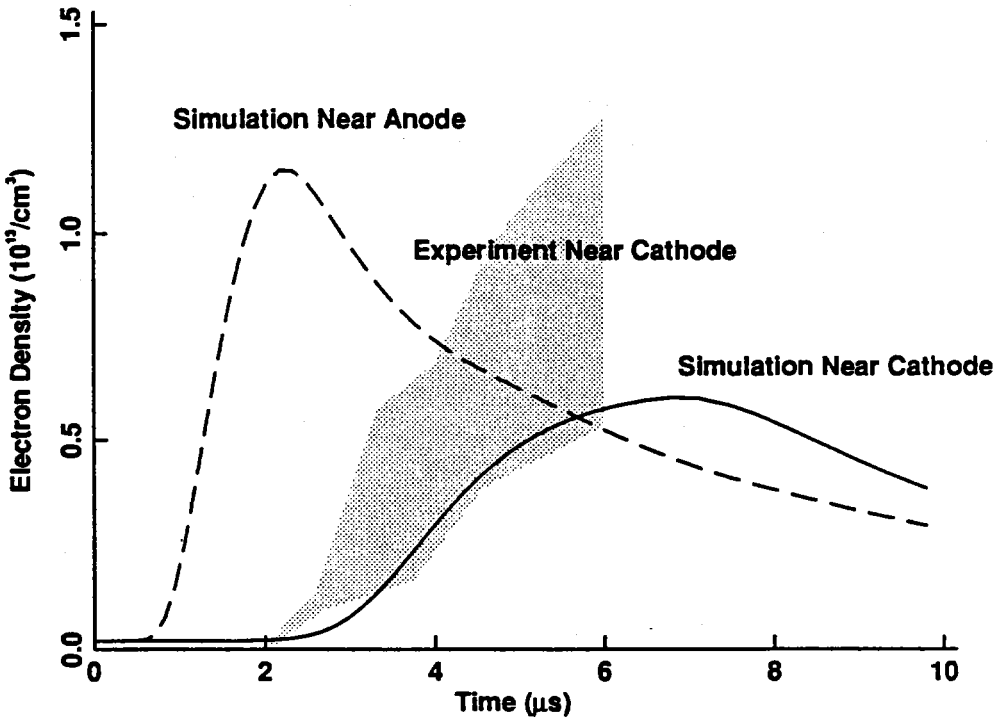

Figure 7 Electron density vs. time at the simulation density probe locations and at one microwave interferometer location. Low density case.

5.2 High Density Case

In order to assess the effects of the fluid pressure, this simulation was run with the inflow density increased by factor of four.

The density contour lines and the velocity field of the plasma at the end of the injection pulse are shown in Figures 8 and 9. They are very similar to the previous case except that the peak density is approximately 4 times higher, and the velocity is slightly greater.

Figures 10 and 11 show the density and velocity at 5 μs. The plasma on field lines near the anode is not bouncing back as much in this simulation, and the mass density is more concentrated.

The electron number density at the simulation density probe locations is plotted versus time in Figure 12. The peak density near the cathode is approximately 4 times as great as in the low density case, while at the anode it is somewhat more than four times as great. Comparison of this figure with Figure 7 shows that the pulse near the anode is somewhat later and its shape somewhat broader in this case.

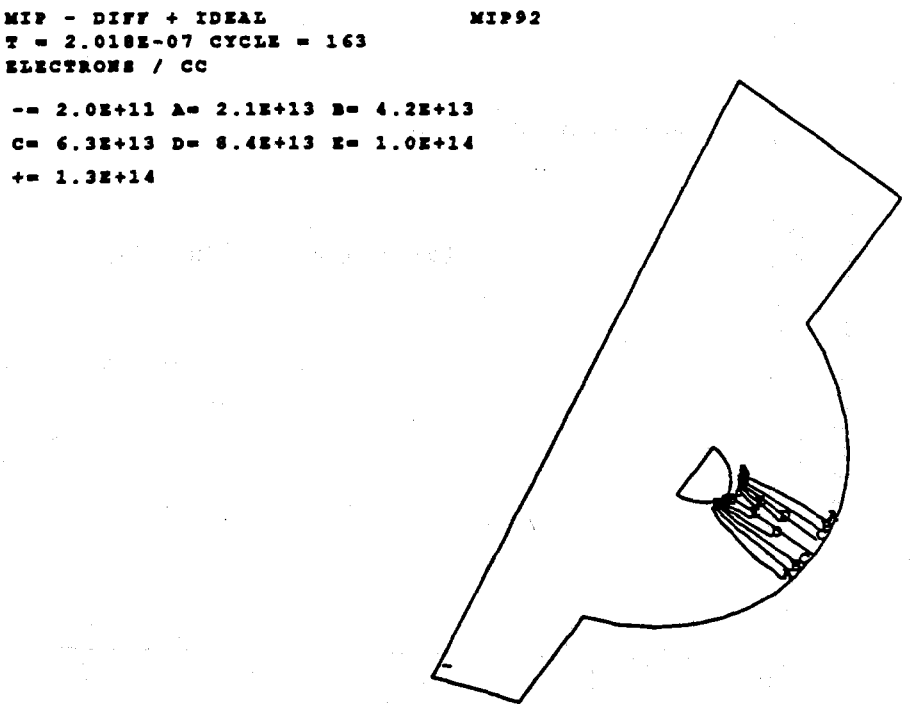

Figure 8 Density at the end of the mass injection pulse. High density case.

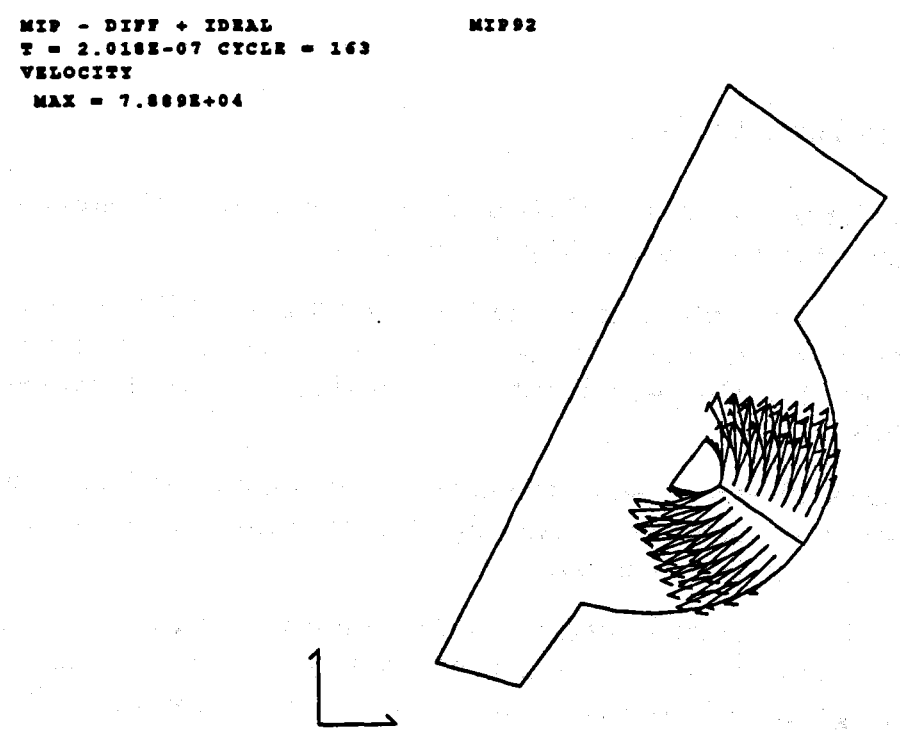

Figure 9 Velocity at the end of the mass injection pulse. High density case.

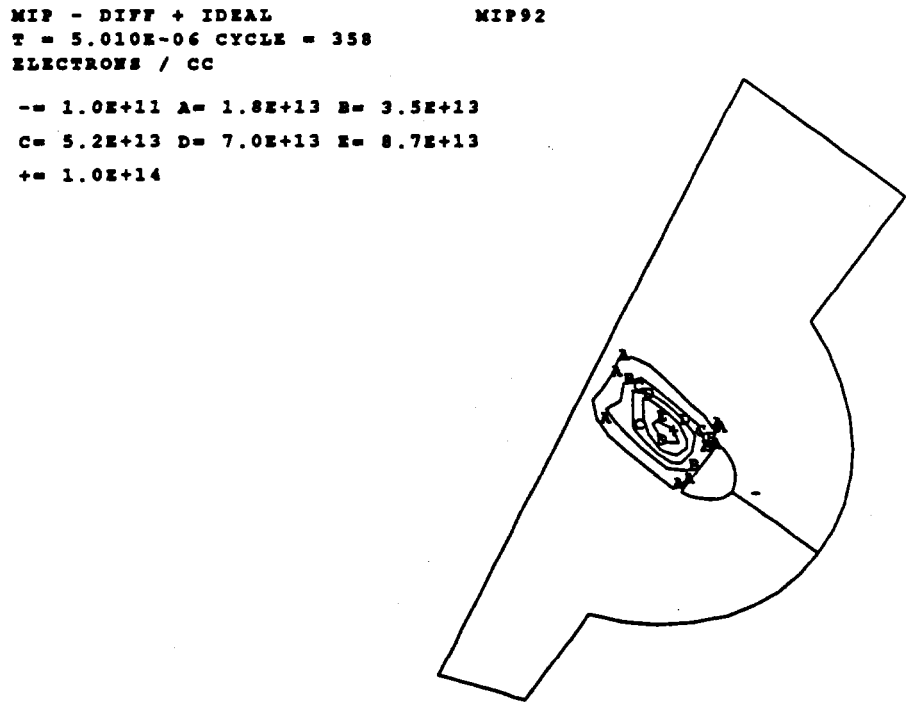

Figure 10 Density at 5 μs after the start of the mass injection pulse. High density case.

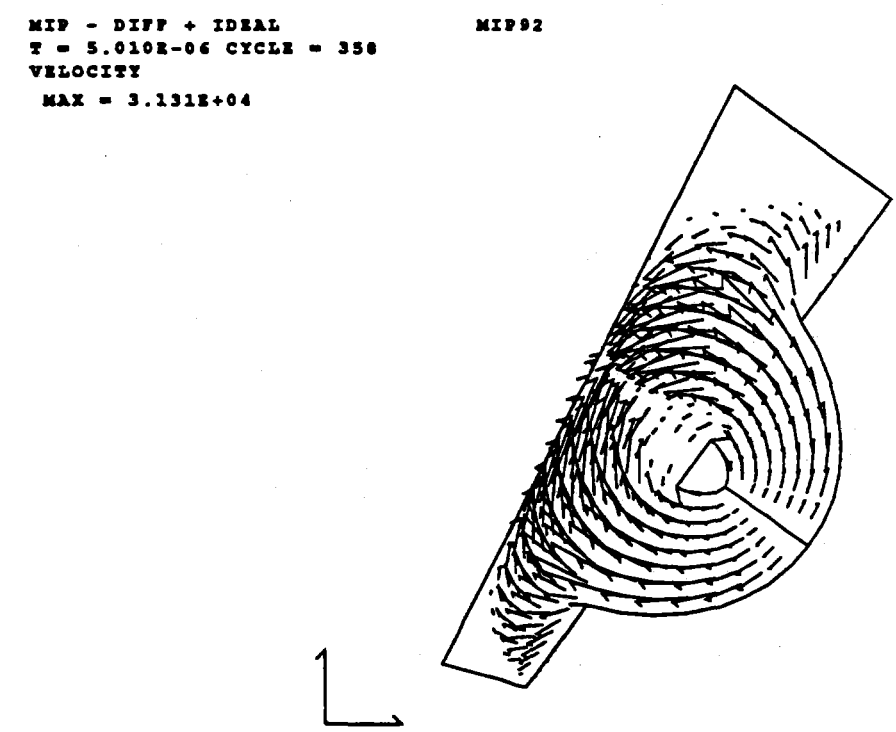

Figure 11 Velocity at 5 μs after the start of the mass injection pulse. High density case.

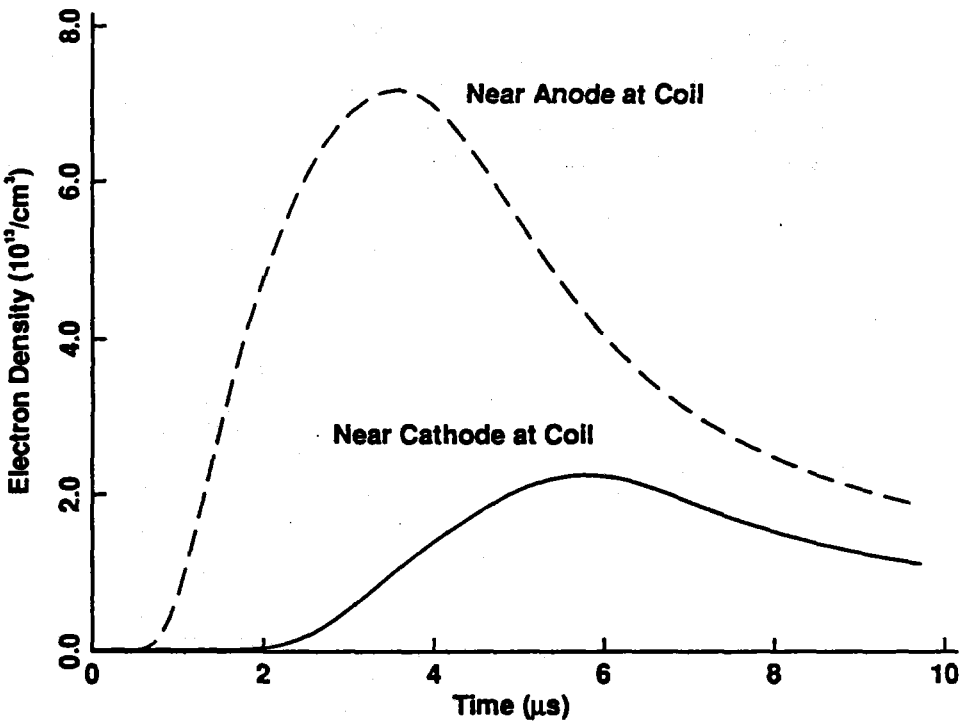

Figure 12 Electron density vs. time at the simulation density probe locations. High density case.

5.3 One-sided Injection Case

Fluid flows in which the internal energy is small compared to the kinetic energy are very similar to free-streaming particle flows. In order to further assess the collisional effects, this simulation was run with the mass inflow from the downstream side of the flashboard suppressed. Since the injected plasma does not collide with its counterpart from the other side of the flashboard, it is not shock heated, and its temperature remains less than 5 eV in the transmission line. The density in the actual experiment in which the two plasmas interpenetrate could be determined by adding the density from this simulation to that from another in which the plasma is injected from the downstream side of the flashboard only. Since the configuration is nearly symmetric, directly between the coil and the cathode, that sum should be approximately twice the density here.

This simulation is of further interest since obstructing the flow from one side of the flashboard is an easy way to lower the mass of the switch plasma. It also could reduce the amount of plasma that might be lost across the field lines toward the load. Since density probe information was not obtained downstream of the coil in these simulations, they do not address that issue.

The density contour lines and the velocity field of the plasma at the end of the injection pulse are shown in Figures 13 and 14. They are very similar to the previous case.

Figures 15 and 16 show the density and velocity at 5 μs. The plasma on field lines near the coil has piled up against the opposite side of the flashboard from which it was emitted. The plasma on field lines near the cathode fills the transmission line. The picture of the density that this gives is significantly different from that of the high density simulation, but not so different from that of the low density one. It is likely that the pressure effects at the higher density render the second of these simulations unreliable as a predictor of the experimental density.

The electron number density at the simulation density probe locations is plotted versus time in Figure 17. It is interesting that the plasma density pulse shape near the cathode differs little from that of either of the previous two simulations.

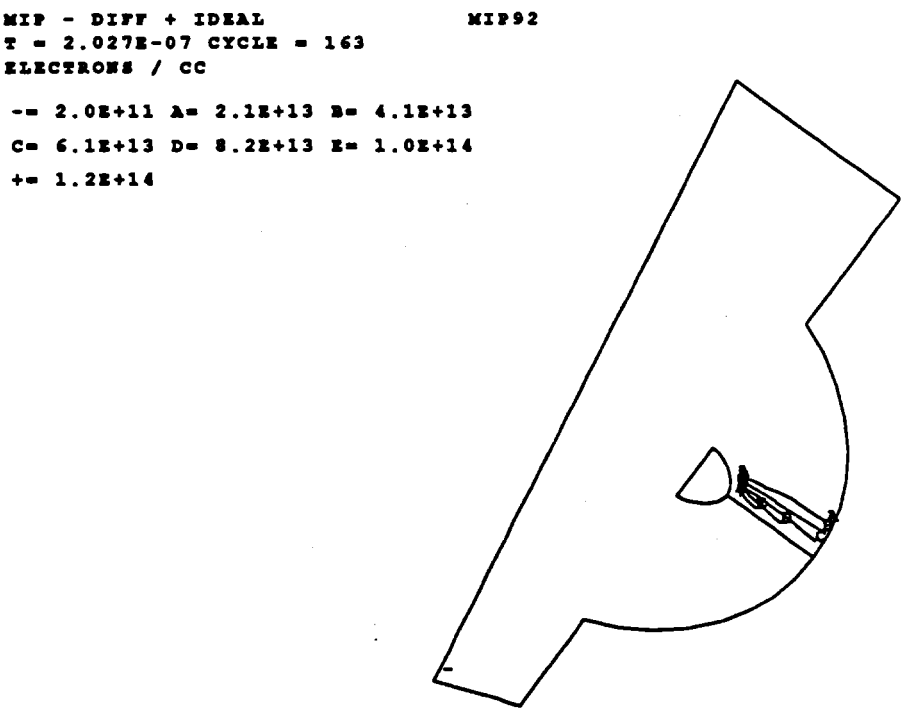

Figure 13 Density at the end of the mass injection pulse. One-sided injection case.

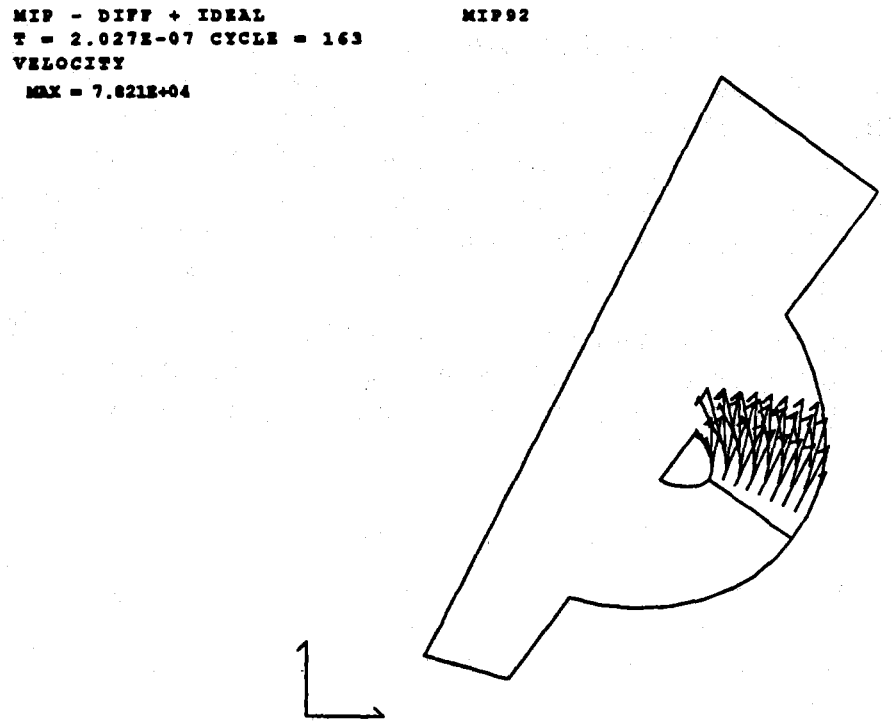

Figure 14 Velocity at the end of the mass injection pulse. One-sided injection case.

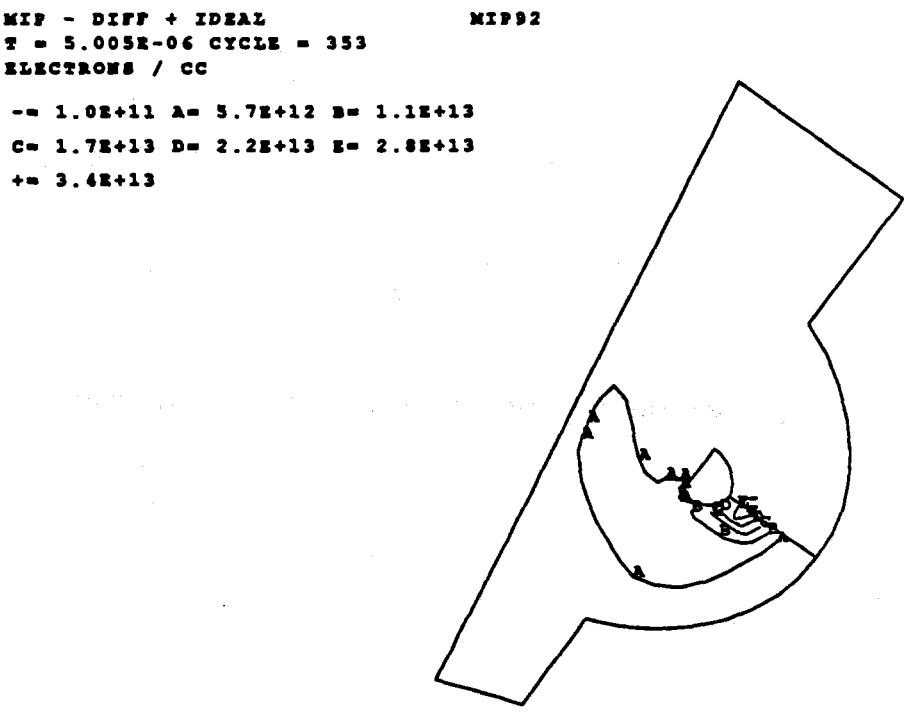

Figure 15 Density at 5 μs after the start of the mass injection pulse. One-sided injection case.

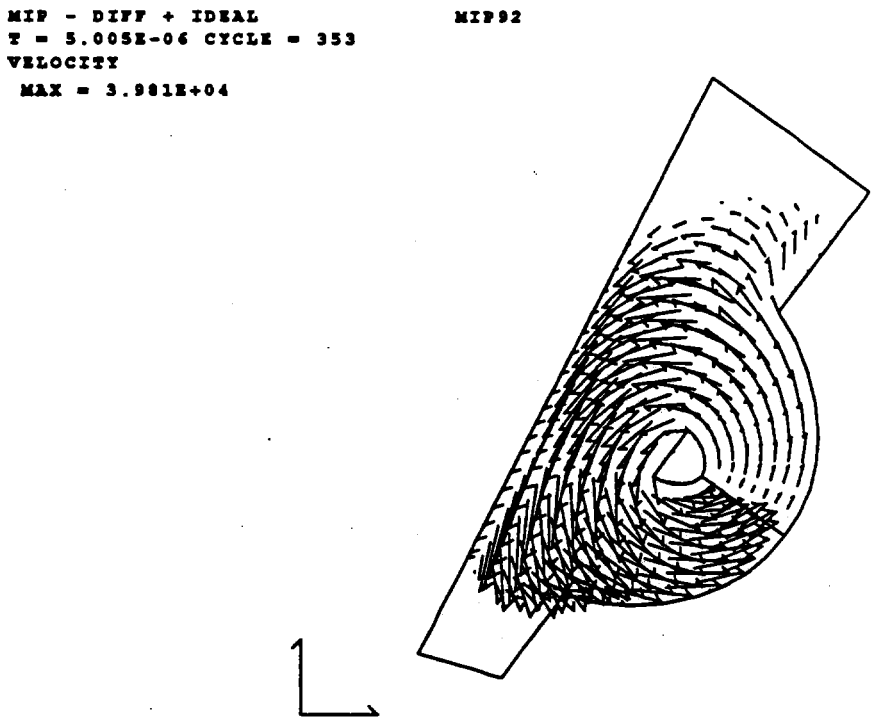

Figure 16 Velocity at 5 μs after the start of the mass injection pulse. One-sided injection case.

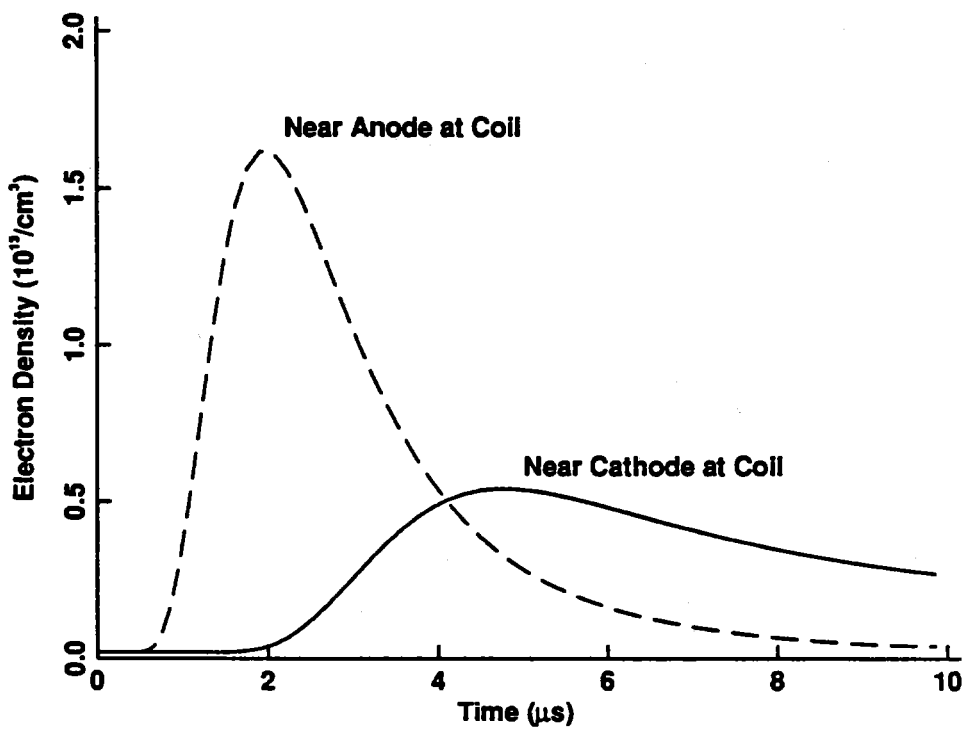

Figure 17 Electron density vs. time at the simulation density probe locations. One-sided injection case.

6. Conclusions and Recommendations

The simulations reported here provide a prediction of the structure and development of the MIP switch plasma during the plasma formation interval. The principle implication for PBFA II is that cathode density measurements may not measure the mass in the switch. The simulations seem to suggest that the total switch mass may rise much faster than the cathode density and begin to fall before the cathode density peaks. If switch mass is an important determinant of switch opening time, using cathode density diagnostics to determine plasma formation time may be misleading.

This simulation model should aid in selection of the plasma formation time for MIP POS shots. The qualitative agreement with experimentally measured plasma densities is sufficiently good that bringing the model into quantiative agreement by adjusting the unknown inflow density and velocity profile seems worthwhile. More simulations similar to these should be run with the density probe locations set the same as those in the experiment to accomplish that.

In order to understand the effect of this plasma distribution and the embedded poloidal field on switch performance, MHD simulations of the plasma during the accelerator power pulse should be performed. MIP POS and current toggle (CT) POS configurations should be simulated both with and without the Hall effect. Present theoretical understanding of the switching mechanism indicates that the Hall effect simulations may be able to produce the first good prediction of CT POS performance. Simulation of the CT POS will require the addition of a magnetic field boundary condition to assure that the fast field coil in the cathode generates the appropriate amount of poloidal field as a function of the toroidal field near that boundary.

References

[1] Michael H. Frese. MACH2: A two-dimensional magnetohydrodynamic simulation code for complex experimental configurations. Technical Report AMRC-R-874, Mission Research Corporation, 1987.

[2] Bruce V. Weber. MIP density measurements at Sandia. Technical Report 89-28, Naval Research Laboratory Plasma Technology Division, September 1989.

Appendix A Historian Change File to Implement Rigid Field Lines in MACH2 v8801

```
*id mhfdif
*dk velbkf
      subroutine velbkf(velx,vely,velz)

c-----project velocity onto vertex magnetic field

cdir$ nolist
*ca common
*ca pointer
cdir$ list

      dimension velx(0:ip2,0:jp2)
      dimension vely(0:ip2,0:jp2)
      dimension velz(0:ip2,0:jp2)

      do 100 j=1,jp1
        do 100 i=1,ip1

          bmag = bvx(i,j)**2 + bvy(i,j)**2 + bvz(i,j)**2

          bdotv =   bvx(i,j) * velx(i,j)
     %            + bvy(i,j) * vely(i,j)
     %            + bvz(i,j) * velz(i,j)

          velx(i,j) = bdotv * bvx(i,j) / ( bmag + 1.e-99 )
          vely(i,j) = bdotv * bvy(i,j) / ( bmag + 1.e-99 )
          velz(i,j) = bdotv * bvz(i,j) / ( bmag + 1.e-99 )

  100 continue

      return
      end

*d magmovc.42
          call bkhntj1(rxnbr,rx,rvolnbr,rcnbr)
          call bkhntj1(rynbr,ry,rvolnbr,rcnbr)
          call bkhntj1(rznbr,rz,rvolnbr,rcnbr)
*d magmovc.44
        call bkntjsc(rbznbr,rbz,rvolnbr,rcnbr)
*id mhfcir
*d circuit.14
      common /ciradd/ vgen,vplas,vcap,current1,oldflux,volts(20),tfire

c-----four choices:
*i circuit.16
```

```
c-----  ident=2: don't change current
c-----  ident=3: solve voltage source circuit equation
*i circuit.75
      elseif( ident .eq. 3 ) then

        if( tfire .lt. 0.0 ) tfire=t

        oldflux = flux
        flux=0.0

        do 500 lblk=1,nblk
c---------magnetic flux (btheta*area) calculated (btheta=bzn)
          call setblk
          call cirflx(flux)
  500   continue

c-------calculate the plasma resistance from
c-------the total joule heating: i.e. de/dt=resis*current**2
        resplas = 2.0*pi*(cirheat-oldcirht)/(dt*amax1(ccrrnt**2,1.e-99))
        oldcirht = cirheat

c-------calculate source voltage
c-------piecewise linear voltage profile
        do 600 k=1,20
          kk=k
          if (timxx(k).gt.(t-tfire)) go to 700
  600   continue
  700   alf = (timxx(kk)-(t-tfire))/(timxx(kk)-timxx(kk-1))
        vgen = alf*volts(kk-1)+(1.-alf)*volts(kk)

c-------calculate plasma voltage
        vplas = resplas * ccrrnt + ( flux - oldflux ) / dt

c-------do differential equations
        vcapnew = vcap + dt * ( current1 - ccrrnt ) / capac
        ccrnew = ccrrnt + 2. * dt * ( vcap - vplas ) / induc1
        curnew = current1 + 2. * dt *
     %                ( vgen - vcap - resis1 * current1 ) / induc1

        vcap = vcapnew
        ccrrnt = ccrnew
        current1 = curnew

*i default.15
      common /ciradd/ vgen,vplas,vcap,current1,oldflux,volts(20),tfire
*i namlst.17
      common /ciradd/ vgen,vplas,vcap,current1,oldflux,volts(20),tfire
*i ttdmped.12
      common /ciradd/ vgen,vplas,vcap,current1,oldflux,volts(20),tfire
*i default.211
      tfire = -1.
```

```
*i namlst.91
     3 ,volts
*d ttdmped.85,88
        if( ident .eq. 0 .or. ident .eq. 1 ) then
          write (unum,151) ccrrnt,idtnpl,inducl,lpnpl,lldtpl,rlnpl
  151     format(' current = ',1pe10.3,' di/dt = ',1pe10.3,
     1          ' lcir = ',1pe10.3,' lpla = ',1pe10.3,/,
     2          ' dl/dt = ',1pe10.3,' plares = ',e10.3)
        else
          write (unum,152) ccrrnt,current1,vgen,vplas,vcap,oldflux
  152     format(' curpla =',1pe10.3,' curgen =',e10.3,' vgen =',
     %           e10.3,' vpla =',e10.3,/,' vcap =',e10.3,' flux =',
     %           e10.3)
        endif

*d bxbybc.46,50
              call bcpntrs(ibdry,this,ghst,this,ghst,all,cell)
              call bcsetvf(bx,by,bxbdy(ibdry,lblk),bybdy(ibdry,lblk))
              call bcmltsc(bx,bx,scrtch(201))
              call bcmltsc(by,by,scrtch(201))
*/ additions for MIP
*i hydmomeq.41

      if( scrtch(202) .eq. 0.0 ) then
        do 350 lblk=1,nblk
          call setblk
          call velbkf(ul,vl,wl)
  350   continue
      endif
*i hydro.79

      if( scrtch(202) .eq. 0.0 ) then
        do 350 lblk=1,nblk
          call setblk
          call velbkf(ul,vl,wl)
  350   continue
      endif
*d remesh.69,83
c-----get new velocities and total momentum from vertex momentum
      do 600 lblk=1,nblk
        call setblk
        call rmshvel(xmom,ymom,zmom)
  600 continue

      if( scrtch(202) .eq. 0.0 ) then
      call bvertx('fine_grd')

c-----fix interior velocity
      do 700 lblk=1,nblk
        call setblk
        call velbkf(u,v,w)
```

```
  700 continue
      endif

c-----fix boundary velocity
      do 800 lblk=1,nblk
        call setblk
        call velbcf(u,v,w)
  800 continue

      do 900 lblk=1,nblk
        call setblk
c-------fix corner velocity
        call velccf(u,v,w)
c-------get internal energy from total energy
        call totnrg2(conserv,rofanom,siecap,m0)
  900 continue
*i hydmomeq.34
        bmult = bmult * scrtch(202)
        dmult = dmult * scrtch(202)
*i hyditblk.82

         sbx(i) = scrtch(202) * sbx(i)
         sby(i) = scrtch(202) * sby(i)
         sbz(i) = scrtch(202) * sbz(i)
*d hyditblk.267,269
          bxl(i,j) = bxl(i,j) + scrtch(202) * dbx(i)
*d hyditblk.267,269
          bxl(i,j) = bxl(i,j) + scrtch(202) * dbx(i)
          byl(i,j) = byl(i,j) + scrtch(202) * dby(i)
          bzl(i,j) = bzl(i,j) + scrtch(202) * dbz(i)
*i cournum.25
        cmag = cmag * scrtch(202)
*d trnspt.62,64
          a = scrtch(202)
          b = 1 - scrtch(202)
          bxn(i,j) =  a * mp(i,j) * bxl(i,j) + b * bxl(i,j)
          byn(i,j) =  a * mp(i,j) * byl(i,j) + b * byl(i,j)
          bzn(i,j) =  a * mp(i,j) * bzl(i,j) + b * bzl(i,j)
*i trnspt.137
          dbxbs = scrtch(202) * dbxbs
*i trnspt.142
          dbybs = scrtch(202) * dbybs
*i trnspt.238
          dbxls = scrtch(202) * dbxls
*i trnspt.243
          dbyls = scrtch(202) * dbyls
*i trnspt.296
          dbzbsp = scrtch(202) * dbzbsp
          dbzbsm = scrtch(202) * dbzbsm
*i trnspt.322
          dbzlsp = scrtch(202) * dbzbsp
```

```
          dbzlsm = scrtch(202) * dbzbsm
*d trnspt.334,336
          a = scrtch(202)
          b = 1 - scrtch(202)
          bxn(i,j) =  a * bxn(i,j) / mp(i,j) + b * bxn(i,j)
          byn(i,j) =  a * byn(i,j) / mp(i,j) + b * byn(i,j)
          bzn(i,j) =  a * bzn(i,j) / mp(i,j) + b * bzn(i,j)
*id mhfhst
*dk fnne
      function fnne(i,j)

c---- compute electron number density in cell i,j

cdir$ nolist
*ca common
*ca pointer
cdir$ list

      fnne = nfe(i,j) * ro(i,j) / ( awc(i,j) * pm )

      return
      end

*i history.12
      external fnne
*d history.44,45
c---------- get ne at first hstnumfc locations
    histf(num) = histvalu( fnne , num)
```

Appendix B MACH2 Input File for MIP Simulation Low Density Case

```
MIP - diff + ideal
 $contrl
   intty = 48htimencyc,10;timestep,10;perform,10;enrgynow,10; ,
   intty(7) = 40hbadcells,10;blank,10;currents 10              ,
   lpr = 1,

   imns = 30,
   twfn = 10.0e-6,
   dt = 1.e-10,
   dto = 0.05e-6,
   dtrst = 1.0e-6,
   dtmax = 1.e-9,

   idealgas = .true.,
       gml = 0.667,

   hydron = .false.,
       omegah = 0.66,
       volratm = 0.9,
       courmax = 1.0,
       rmvolrm = 0.2,
       mu = 5.6,
   rad = 6hdirtyh ,
       fox = 0.1,
   ciron = .false.,
   thmldif = .false.,
       flxlmt = 0.04,
   meshon = .false.,
       nsmooth = 4,
       wrelax = 0.25,
   brbzon = .true.,
   magon = .true.,
       itpot = 20,
       potrelx = 0.5,
   bdiff = .true.,
      joultmlt = 0.,
      multgrd = .true.,
      mgmode = 8hconverge,
      rdtol = 1.e-4,
      cntrmin = 1.0,

   scrtch(201) = 2.64,
   scrtch(202) = 0.,

   nhist=5,
```

```
 fdycupr= 1.91e-4,
 hstnumfc = 4,
 histnum = 4,

     histx(1) = 0.2134, histy(1) = 0.2992,
     histx(2) = 0.2599, histy(2) = 0.2646,
     histx(3) = 0.2521, histy(1) = 0.3875,
     histx(4) = 0.3186, histy(2) = 0.3407,

 rof = 1.e-9,
 aresvac = 100.,
 rofanom = 1.5e-9,

 plot(7) = 8hdiffusiv ,

$end
$curnt

 ident = 3,
 capac = 4.e-10,
 induc1 = 100.e-9,
 resis1 = 4.4,

timxx( 1)= 0.         , 0.3007e-07, 0.3674e-07, 0.4342e-07, 0.5010e-07,
timxx( 6)= 0.7012e-07, 0.7680e-07, 0.8348e-07, 0.9015e-07, 0.9683e-07,
timxx(11)= 0.1168e-06, 0.1435e-06, 0.1502e-06, 0.1569e-06, 0.1635e-06,
timxx(16)= 0.1702e-06, 0.1769e-06, 0.1836e-06, 1.e-3,

volts(1)  =  0.00e+00,  6.84e+04,  1.57e+05,  6.38e+05,  2.23e+06,
volts(6)  =  1.07e+07,  1.20e+07,  1.22e+07,  1.16e+07,  1.06e+07,
volts(11) =  4.66e+06, -1.85e+06, -3.24e+06, -3.80e+06, -3.56e+06,
volts(16) = -2.76e+06, -1.98e+06,  3.06e+06,  3.06e+06,

$end
$ezgeom

   npnts = 20,
   pointx(1) = 0.2914, pointy(1) = 0.4757,
   pointx(2) = 0.3801, pointy(2) = 0.4104,
   pointx(3) = 0.2521, pointy(3) = 0.3975,
   pointx(4) = 0.3286, pointy(4) = 0.3407,
   pointx(5) = 0.2132, pointy(5) = 0.3201,
   pointx(6) = 0.2776, pointy(6) = 0.2722,
   pointx(7) = 0.1980, pointy(7) = 0.2898,
   pointx(8) = 0.2577, pointy(8) = 0.2454,
   pointx(9) = 0.1590, pointy(9) = 0.2123,
   pointx(10) = 0.2066, pointy(10) = 0.1770,
   pointx(11) = 0.1243, pointy(11) = 0.1434,
   pointx(12) = 0.1713, pointy(12) = 0.1296,
   pointx(13) = 0.2866, pointy(13) = 0.2576,
   pointx(14) = 0.3511, pointy(14) = 0.2690,
```

```
   pointx(15) = 0.2855, pointy(15) = 0.2455,
   pointx(16) = 0.3318, pointy(16) = 0.2111,
   pointx(17) = 0.2742, pointy(17) = 0.2410,
   pointx(18) = 0.2822, pointy(18) = 0.1762,
   pointx(19) = 0.2855, pointy(19) = 0.2455,
   pointx(20) = 0.3318, pointy(20) = 0.2111,

   nblk = 9,
   corners(1,1) = 1,2,4,3,
   corners(1,2) = 3,4,6,5,
   corners(1,3) = 4,14,13,6,
   corners(1,4) = 14,16,15,13,
   corners(1,5) = 5,6,8,7,
   corners(1,6) = 7,8,10,9,
   corners(1,7) = 8,17,18,10,
   corners(1,8) = 17,19,20,18,
   corners(1,9) = 9,10,12,11,

   numarcs = 8,
   arctype(1) = 7h2pt&dir ,
   arctype(2) = 7h2pt&dir ,
   arctype(3) = 7h2pt&dir ,
   arctype(4) = 7h2pt&dir ,
   arctype(5) = 7h2pt&dir ,
   arctype(6) = 7h2pt&dir ,
   arctype(7) = 7h2pt&dir ,
   arctype(8) = 7h2pt&dir ,
   arcs(1,1) = 14,4 , 0.5080,
   arcs(1,2) = 14,16,-0.4920,
   arcs(1,3) = 13, 6, 0.5918,
   arcs(1,4) = 13,15,-0.4082,
   arcs(1,5) = 18,20, 0.0846,
   arcs(1,6) = 18,10,-0.9154,
   arcs(1,7) = 17,19, 0.0014,
   arcs(1,8) = 17, 8,-0.9986,

$end
$ezphys
    ang = 2.,
    awg = 12.,
    gdvlg = 0.,
    roig = 2.e-9,
    tempig = 0.025,
    icellsg = 8,
    jcellsg = 8,
    matnameg = 1hc ,
    eta0g = 2.5e4,
    atamaxg = 1.,
    dirintpg = 7hintp3t1,
$end
$inmesh
```

```
name(5) = 8hmip92    ,
name(6) = 8h         ,
nigen = 0,
niter = 1,
eqvol = 0.,
siecap = 3.2482e11,
vfqctim = -0.05e-6,

   ibcseq(1,1) = 1,3,2,4,

      magxybc(1,1) = 8hconductr,
      magzbc(1,1) = 8hinsulatr,
          currcir(1,1) = 1,
      hydbc(1,1) = 8hflowthru,
          roflow(1,1) = 1.e-9,
          tflow(1,1) = 0.025,
          eflow(1,1) = 9.04e5,
          pflow(1,1) = 6.03e-4,

   ibcseq(1,2) = 1,3,2,4,

   ibcseq(1,3) = 1,3,2,4,
   icells(3) = 4,
       magxybc(3,3) = 8hspecfied,
           bxbdy(3,3) =  0.5247,
           bybdy(3,3) = -0.8513,

   ibcseq(1,4) = 1,3,2,4,
   icells(4) = 4,
       magxybc(3,4) = 8hspecfied,
           bxbdy(3,4) = -0.0905,
           bybdy(3,4) = -0.9959,

      magxybc(2,4) = 8hsymmetry,
      potbc(2,4) = 8htdotgphi,
      hydbc(2,4) = 8hflowthru,
      velbc(2,4) = 6hpulsed,
          roflow(2,4) = 5.e-7,
          tflow(2,4) = 1.0,
          eflow(2,4) = 3.62e7,
          pflow(2,4) = 2.41e-1,
          uflow(2,4) = 6.e4,
          vflow(2,4) = 8.e4,

    jcells(5) = 4,
    ibcseq(1,5) = 1,3,2,4,
        magxybc(2,5) = 8hspecfied,
            bxbdy(2,5) = 0.5962,
            bybdy(2,5) = 0.8029,

    ibcseq(1,6) = 1,3,2,4,
```

```
      ibcseq(1,7) = 1,3,2,4,
      icells(7) = 4,
          magxybc(1,7) = 8hspecfied,
              bxbdy(1,7) = -0.9662,
              bybdy(1,7) =  0.2577,

      ibcseq(1,8) = 1,3,2,4,
      icells(8) = 4,
          magxybc(1,8) = 8hspecfied,
              bxbdy(1,8) = -0.9290,
              bybdy(1,8) = -0.3700,
         magxybc(2,8) = 8hsymmetry,
         potbc(2,8) = 8htdotgphi,
         hydbc(2,8) = 8hflowthru,
         velbc(2,8) = 6hpulsed,
             roflow(2,8) = 5.e-7,
             tflow(2,8) = 1.0,
             eflow(2,8) = 3.62e7,
             pflow(2,8) = 2.41e-1,
             uflow(2,8) = -6.e4,
             vflow(2,8) = -8.e4,

      ibcseq(1,9) = 1,3,2,4,

         magxybc(3,9) = 8hconductr,
         hydbc(3,9) = 8hflowthru,
             roflow(3,9) = 1.e-9,
             tflow(3,9) = 0.025,
             eflow(3,9) = 9.04e5,
             pflow(3,9) = 6.03e-4,

   velcc(3,1) = 7hproject ,

   velcc(2,2) = 7hproject ,
   velcc(3,2) = 7hproject ,

   velcc(1,3) = 7hproject ,
   velcc(4,3) = 7hproject ,

   velcc(2,5) = 7hproject ,
   velcc(3,5) = 7hproject ,

   velcc(2,6) = 7hproject ,
   velcc(3,6) = 7hproject ,

   velcc(1,7) = 7hproject ,
   velcc(4,7) = 7hproject ,

   velcc(2,9) = 7hproject ,

$end
```

```
$modtim

  tmod = 1.0e-7,

$end
$contrl

  dtmax = 1.,
  hydron = .true.,
  courmax = 1.,
  bdiff = .false.,

$end
$modtim

  tmod = 2.0e-7,

$end
$contrl

  dto = 0.50e-6,

$end
$inmesh

   velbc(2,4) = 8hfreeslip ,
   probc(2,4) = 4hwall ,

   velbc(2,8) = 8hfreeslip ,
   probc(2,8) = 4hwall ,

 $end
```

Distribution:

Maxwell Laboratory (3)
Attn: Bill Rix
John Shannon
Michael Coleman
8888 Balboa Avenue
San Diego, CA 92123

S-Cubed (4)
Attn: Andrew Wilson
Eduardo Waisman
Paul Steen
Don Parks
P. O. Box 1620
La Jolla, CA 92038

Naval Research Laboratory
Attn: Gerry Cooperstein
Code 4770
4555 Overlook Ave. SW
Washington, DC 20375

Naval Research Laboratory (7)
Attn: Paul Ottinger
John Grossman
Bob Commisso
Dave Mosher
Jesse Neri
Bruce Weber
Dave Hinshelwood (Jaycor)
Code 4771
4555 Overlook Ave. SW
Washington, DC 20375

Seishi Hamasaki
Jason Associates
2002 Jimmy Durante Blvd.
Suite 314
Del Mar, CA 92014

Krall Associates
Attn: Nick Krall
1070 America Way
Del Mar, CA 92014

Lawrence Livermore Nat. Lab
Attn: Dennis Hewett
MS L472
P. O. Box 808
Livermore, CA 94550

Los Alamos Nat. Laboratory (2)
Attn: Rod Mason
Dan Winske
MS E-531
P. O. Box 1663
Los Alamos, NM 87545

Cornell University (3)
Laboratory of Plasma Science
Attn: Ravi Sudan
John Greenly
Lynne Adler
369 Upson Hall
Ithaca, NY 14853

University of New Mexico (2)
Dept. of Chem. & Nuc. Eng.
Attn: Norm Roderick
James Nicholson
Albuquerque, NM 87131

University of New Mexico
Department of Electrical Engineering
Attn: Edl Schamiloglu
323C EECE Building
Albuquerque, NM 87131

Mission Research Corporation (2)
Attn: Joe Kindel
Erick Lindman
127 Eastgate Drive, Suite 208
Los Alamos, NM 87544

Mission Research Corporation (2)
Attn: Bob Peterkin
Steve Payne
1720 Randolph Road, SE
Albuquerque, NM 87106

Numerex
Attn: Mike Frese
1400 Central SE
Albuquerque, NM 87106

Defense Nuclear Agency
RAEV
Attn: Capt. Jerry Fisher
6801 Telegraph Road
Alexandria, VA 22310

Berkeley Research Associates (2)
Attn: Steve Brecht
Bob Kares
P. O. Box 241
Berkeley, CA 94701

Air Force Academy
Attn: Capt. Robert Lawconnell
FJSRL/NH
Colorado Springs, CO 80840

Yale University
Dept. of Applied Physics
Attn: Philippe Simiion
P. O. Box 2157
Yale Station
New Haven, CT 06520-2157

Roger Bengston
411 Honeycomb Ridge
Austin, TX 78746

PSI
Attn: Ian Smith
Laslo Dimenter
Kurt Neilsen
600 McCormick Street
San Leandro, CA 94577

Physics International
Attn: John Goyer
Peter Sincerny
David Kortbawi
2700 Merced Street
San Leandro, CA 94577

1200	J. P. VanDevender
1241	J. R. Freeman
1242	B. N. Turman
1260	D. L. Cook
1262	L. P. Mix
1263	D. H. McDaniel
1263	C. W. Mendel, Jr.
1263	W. B. S. Moore
1263	G. E. Rochau
1263	M. E. Savage
1263	H. N. Woodall
1263	D. M. Zagar
1264	R. W. Stinnett
1264	T. J. Renk
1265	J. P. Quintenz
1265	M. P. Desjarlais
1265	S. E. Rosenthal
1265	S. A. Slutz
1265	M. A. Sweeney (6)
1267	G. Cooper
1267	W. A. Stygar
1270	J. K. Rice
1271	G. O. Allshouse
1271	T. W. Hussey
1272	G. W. Kuswa
1272	J. E. Bailey
1275	J. R. Woodworth
1290	T. H. Martin
3141	S. A. Landenberger (5)
3141-1	C. L. Ward (8) for DOE/OSTI
3151	W. I. Klein (3)
8524	J. A. Wackerly